Received: 15 November 2024 | Revised: 20 January 2025 | Accepted: 25 January 2025

DOI: 10.1002/pc.29617

RESEARCH ARTICLE

spe INSPIRING PLASTICS PROFESSIONALS Polymer COMPOSITES WILEY

Mechanical properties and predictive analysis of multi-material polypropylene-glass fiber sandwich structures produced by material extrusion

Julia Utz[1] | **Amelie Ferbert**[1] | **Nico Geis**[2] | **Holger Ruckdäschel**[1,2]

[1]Department of Polymer Engineering, University of Bayreuth, Bayreuth, Germany

[2]Neue Materialien Bayreuth GmbH, Bayreuth, Germany

Correspondence
Julia Utz, Department of Polymer Engineering, University of Bayreuth, Universitätsstrasse 30, 95447, Bayreuth, Germany.
Email: julia.utz@uni-bayreuth.de

Funding information
Universität Bayreuth

Abstract

Combining multiple filaments in material extrusion (MEX) to tailor mechanical properties is increasingly significant in science and applications. However, understanding the interaction between different materials, the influence on the mechanical properties and the predictability of such properties is still poor. Therefore, this study investigates the tensile and flexural behavior of 3D-printed sandwich-type composites made of polypropylene (PP) and glass fiber-filled polypropylene (PPGF). The materials exhibit different mechanical properties, with PP being more ductile and flexible and PPGF being more brittle and stiff. Various contents of PP and PPGF were used. Measured mechanical values were correlated with theoretical predictions. The tensile properties scaled linearly with the material composition, covering a range of moduli and strength values between 500–2910 MPa and 18–43 MPa, respectively. A rule of mixture could be applied, although PPGF layers tended to crack early. The ductile nature of PP allowed for bridging cracks, preventing premature failure. In flexural tests, the shell material dominated modulus, strength and failure mode. The samples with PPGF shells failed by cracking, while specimens with PP shells showed high deformation without clear failure. By varying contents and layer order, flexural moduli ranging from 680 to 3180 MPa and flexural strengths from 25 to 65 MPa were reached. Additionally, the study demonstrated that theoretical calculations and predictions of tensile and flexural moduli were highly accurate with an average deviation of 6.0% and 1.4%, respectively. This highlights the potential for tailoring mechanical properties based on the characteristics of PP and PPGF.

Highlights

- High PP/PPGF interface adhesion ensures reproducible multi-material printing.
- Whole range of mechanical properties from ductile PP to stiff PPGF is reached.
- Order and amount of both materials determine failure behavior.
- Analytical prediction of modulus is very accurate.

KEYWORDS
fused filament fabrication, mechanical properties, multi-material, polypropylene, prediction, sandwich

1 | INTRODUCTION

Multi-material-printing is one concept in additive manufacturing to customize functionality by a combination of different materials. Various AM technologies are used for this purpose, including vat photopolymerization,[1,2] powder bed technology,[3] material jetting (MJ),[4,5] direct ink writing (DIW)[6,7] and material extrusion (MEX).[6,8]

The multi-material printing technology used in this study is fused filament fabrication (FFF), which belongs to the MEX category. The principle behind multi-material FFF is to incorporate different thermoplastic filaments within one part and print job. Different printer concepts exist to realize the combination of multiple filaments. One approach involves a single nozzle to which all filaments are fed. In such a single extruder system, mixing elements can help to achieve different material compositions of the individual filament materials.[9] The more prevalent and commercially used concept is a printing head equipped with multiple nozzles, one for each filament. A study by Baca et al. compared both concepts and found no significant difference in the mechanical properties of samples printed either with single- or multi-material configuration.[10]

Multi-material FFF is frequently used for printing visual patterns, prototypes or toys that require multiple colors. Another common approach is combining the actual product material with a support material, which can be removed after the completion of the print job.[11] However, these applications represent only a fraction of the possibilities that arise from combining materials with diverse properties. Further examples include combining mechanical properties, distinct thermal or mechanical conductivity, or biological functionality.[12] This study's primary focus is tailoring mechanical properties using different filament materials. Several publications have already addressed this topic, examining various aspects related to materials, processing parameters and joining geometry. A brief overview is given below.

A basic design involves printing a sandwich-type structure using two or three distinct thermoplastics. It has to be considered that the term "sandwich" is used in various contexts. From a mechanical point of view, a sandwich structure typically consists of stiff face sheets combined with a relatively "soft" core, designed to achieve high stiffness at low weight.[13,14] Other layered structures are often referred to as composites or hybrids. The term "hybrid" also lacks a clear definition. Most refer to it as a mixture on the submicron level. A publication by Nanko proposes a new classification that distinguishes between structurally hybridized materials, materials hybridized in chemical bonds and functionally-hybridized materials. In this classification, macroscopic stacking of different layers falls into the first category.[15] In the context of additive manufacturing, the term sandwich is often used to describe the geometrical arrangement of stacked layers made from different materials. While this usage differs from the traditional definition, many of the mechanical assumptions for calculations still apply (for details, see section 2.4). Therefore, this work retains the term sandwich to describe these structures.

Arifvianto et al. printed a combination of polylactic acid (PLA) and thermoplastic polyurethane (TPU) filament. They showed that a hybrid behavior between both materials could be achieved regarding tensile strength and modulus.[16] An interesting observation of this group was that TPU could prevent premature fracture of samples, even after the elongation at break of PLA was reached. However, it was noted that the PLA and TPU exhibit low adhesion. Better adhesion was observed in the PLA/copper powder-doped PLA layered structure investigated by Yilmaz et al. They demonstrated that the tensile and flexural properties of multi-material prints with a PLA core and a PLA-copper shell resulted in intermediate values for modulus and strength.[17]

Another sandwich structure was investigated by Baca et al.[10] They used a triple combination of acrylonitrile butadiene styrene (ABS), TPU and high-impact polystyrene (HIPS). They also observed intermediate tensile strength for combinations of two or all three materials but did not elaborate on the failure mechanisms. A similar study was conducted by the same group on PLA-ABS-HIPS composites.[9] Another paper by Kim et al. investigated the tensile strength of PLA-ABS composites.[18] In contrast to the previously mentioned publications, they vertical stacked the two materials and demonstrated that the PLA-ABS interface was the weak point of all samples.

Since the interface between different filament materials is always a critical aspect, some other publications specifically address this issue and measures to improve adhesion. The group of Lopes studied the effect of different printing parameters on the tensile strength of samples made of polyethylene terephthalate (PET), PLA, TPU and composites with zebra-crossing structures. In

comparison to continuously printed samples, the zebra-like tensile bars exhibited significantly lower tensile strength, while the modulus decreased only slightly.[19]

Rabbi et al. worked with a combination of PLA and PA. They focused on a new testing approach to determine the adhesion between the two materials. Similar to testing fiber composites, they designed a bending beam with an initial crack to calculate energy dissipation and evaluate crack propagation at the interface between both thermoplastics. They showed that different printing parameters such as extruder temperature, printing orientation and speed affect the crystallinity as well as the defect density of the sample, leading to changes in adhesion.[20] In two other publications, temperature was identified as the most important parameter affecting adhesion. A study by Yin et al. investigated the influence of extruder temperature, printing bed temperature, and printing speed on the joining temperature of ABS-TPU combinations. Using temperature sensors in the joining area, they demonstrated that reheating the adjacent layers above the glass transition temperature (T_g) is necessary to enable good adhesion between the two materials.[21] Lin et al. also investigated the influence of temperature on entanglement and adhesion of PLA and polycaprolactone (PCL). They employed a single-layer temperature adjustment method to address the issue of vastly different processing temperatures of 110 and 210°C. An intermediate temperature of 130°C proved to be suitable for a good adhesion between PLA and PCL.[22] In addition to various processing parameters, variation of the joining geometry is also an approach to improve adhesion. Several studies investigated different joining angles and more complex joining geometries such as U-shape, dovetail and encapsulation.[23–25]

Many of the previously mentioned studies have found that the Young's modulus falls within an intermediate range between the moduli of the individual components, especially for sandwich-type structures. Nevertheless, these observations were primarily qualitative and have not been validated with theoretical models. From a design standpoint, it would be interesting if printed multi-material sandwiches could be calculated based on the individual material amounts, enabling the prediction of multi-material mechanics. Some publications deal with calculations for printed parts based on classical laminate theory (CLT). Since printed layers behave similarly to fiber composite layers, Mishra et al. and Nasirov et al. showed that CLT is suitable for the prediction of the mechanical behavior of printed PLA parts.[26] However, Mishra et al. also noted that the calculations are not perfect for multi-material prints of PLA and carbon fiber-reinforced PLA due to lower adhesion and the occurrence of defects.[27] Works examining the validity of theoretical models for the mechanical properties of multi-material prints are scarce.

In general, multiple theoretical models have been reported for predicting the mechanical properties of multi-material systems. A simple approach derived from fiber composites is the rule of mixture. This concept estimates the Young's modulus by considering the moduli and volume fractions of the individual materials arranged in parallel to the load direction. Taking a step further, stacking multiple composite layers with different orientations or compositions, the above-mentioned CLT can be applied. Other multi-material systems are known from sandwich structures, where shell layers are combined with another core material for lightweight purposes. While all of these theories have relevance to multi-material printing, they are rarely used to predict the mechanical properties of 3D printed samples.[28,29]

Summarizing the previous work on multi-material FFF printing, some general findings emerge:

1. Combinations of stiff and soft/flexible materials are used to tailor the mechanical properties of printed samples.
2. Good adhesion between the respective materials is crucial for achieving high tensile strength and modulus in printed parts. Adhesion presents challenges arising from physical (diffusion, mobility on chains) and chemical (different materials) aspects.
3. While mechanical properties of multi-material prints are often measured, a systematic investigation of failure mechanisms and prediction of composite properties are lacking.

Considering these aspects, the current study aims to deepen the understanding of the mechanical properties of multi-material 3D-printed structures. Unlike previous studies, which mostly rely on combining entirely different materials for stiff-soft combinations, this work pairs neat polypropylene (PP) with its glass-fiber-reinforced variant. This approach offers a key advantage: the shared polymer matrix ensures high chemical affinity, eliminating adhesion issues and enabling precise analysis of mechanical behavior. At the same point, the addition of glass fibers enables a sufficient increase in modulus and tensile strength. Studies, where neat PP filaments and glass fiber-filled ones were extruded and printed, showed that PP-glass fiber printed parts showed up to 12 times higher modulus and 60% higher strength than their unfilled counterparts.[30–32]

The current study uses the favorable precondition, PP-PPGF combinations provide and explores the tensile and flexural behavior of sandwich-layered composites,

TABLE 1 Mechanical properties for printed polypropylene (PP)[33] and glass fiber-filled polypropylene (PPGF)[34] according to data sheets (100% Infill, printed laying flat on the printing bed).

Property	PP	PP-GF
Tensile strength (MPa)	15.5	41.7
Elongation at break (%)	>119	4.4
Young's modulus (MPa)	541	2628
Flexural strength (MPa)	229	76.8
Flexural modulus (MPa)	575	3507
Flexural strain at break (%)	9.4	4.6

focusing on how the composition and arrangement of layers influence mechanical performance and failure mechanisms. These results are compared with theoretical predictions, addressing the notable gap in accurate predictive models for multi-material 3D printing. This offers valuable new insights paving the way for improved modeling in additive manufacturing.

2 | EXPERIMENTAL MATERIALS AND METHODS

2.1 | Materials

Two 3D printing filaments from BASF 3D Printing Solutions GmbH (Heidelberg, Germany) with a diameter of 2.85 mm were used in this study. The first filament is Ultrafuse PP Natural (PP), an unfilled PP type. The second filament is Ultrafuse PP-GF30 (PPGF), which is a PP filled with 30 wt% glass fibers. The materials exhibit significant differences in their mechanical properties which was crucial for interpreting the influence of composition on the mechanical properties of the sandwich-type structures. The mechanical properties, according to the data sheets, are given in Table 1.

2.2 | Printing

All specimens were fabricated via FFF using an Ultimaker S5 printer (Ultimaker, Utrecht, Netherlands). The dual-nozzle print head was equipped with a AA0.4 print core for PP and a CC0.4 print core for PPGF. The CC nozzles differ from the AA nozzles as they possess a wear-resistant coating, making them particularly suitable for printing abrasive filaments. The Ultimaker Air Manager attachment enabled more reliable printing using a closed build chamber. An Ultimaker Adhesion Sheet on the glass printing bed improved the adhesion between PP and the plate. The printing parameters are listed in Table 2. Ultimaker Cura software was used for slicing.

TABLE 2 Printing parameters for all samples.

Parameter	Value
Layer height (mm)	0.1
Build plate temperature (°C)	100
Printing speed (mm/s)	45
Nozzle temperature (PP) (°C)	230
Nozzle temperature (PPGF) (°C)	235
Infill degree (%)	100
Infill pattern	Lines (±45°)
Wall line count	3
Top/bottom layer count	3

Two geometries were printed. For tensile testing, standard 1A dog bone specimens were produced according to DIN EN ISO 527. For flexural tests, bars with dimensions of 80 mm length, 10 mm width and 4 mm height according to DIN EN ISO 178 were used. All samples were printed lying flat on the building plate with an infill density of 100% and an infill pattern with 45°/−45° lines. A layer height of 0.1 mm was used, resulting in a layer count of 40 for all samples. Pure PP and PPGF samples were printed, as well as six different symmetrical sandwich-type structures. Table 3 summarizes all compositions and respective abbreviations used in the manuscript. Figure 1 illustrates the orientation of a tensile bar on the printing bed and the layer structure of all eight sample types.

2.3 | Characterization

The structure and layer composition of the printed samples were investigated by light microscopy. For this purpose, printed tensile bars were cut in the middle perpendicular to the layer orientation, embedded in resin, and polished. The cross-sectional area was analyzed using a Keyence VR5200 (Keyence Corporation, Osaka, Japan). Qualitative evaluations were made regarding layer adhesion and porosity.

The mechanical properties were tested under tensile and flexural loads. Tensile testing was performed according to DIN EN ISO 527 on a Zwick Z1485 universal testing machine (ZwickRoell, Germany). Young's modulus was measured at a testing speed of 1 mm/min up to 0.25% of elongation, continuing the measurement

TABLE 3 List of printed samples with composition and order of layers (shell material always named first).

Name	Amount of PP (vol%)	Amount of PPGF (vol%)	Shell layer
100PP	100	0	PP
75PP-25PPGF	75	25	PP
50PP-50PPGF	50	50	PP
25PP-75PPGF	25	75	PP
100PPGF	0	100	PP-GF
75PPGF-25PP	25	75	PP-GF
50PPGF-50PP	50	50	PP-GF
25PPGF-75PP	75	25	PP-GF

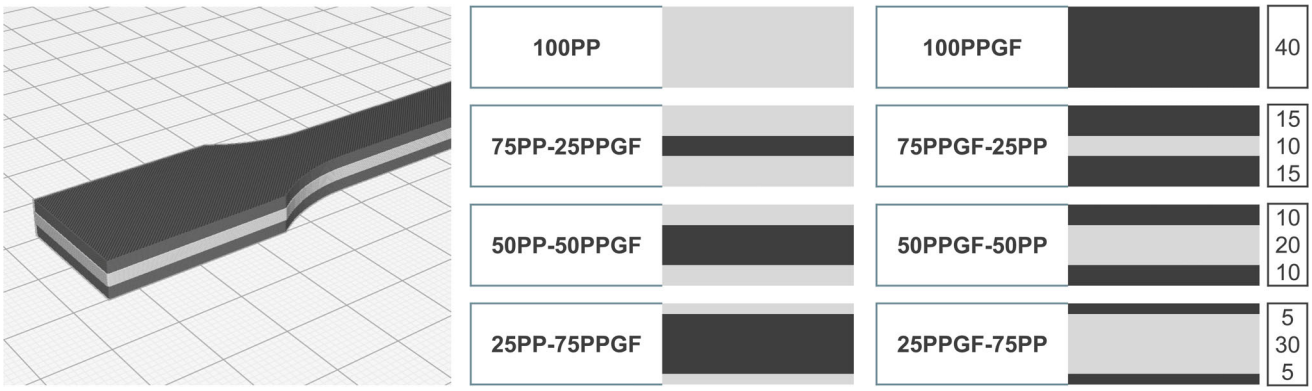

FIGURE 1 Illustration of layer structure of sandwich-type samples with different compositions. The numbers on the right are layer counts.

with 50 mm/min. 3-point-flexural tests were carried out in accordance with DIN EN ISO 178 on a Zwick Z2.5 universal testing machine (ZwickRoell, Germany) at a testing speed of 3 mm/min with a support spacing of 64 mm. For each material composition, at least five specimens were used for both the tensile and flexural tests.

2.4 | Theoretical basics of the calculation of tensile and flexural mechanical properties of sandwich structures

In this study, different multi-material prints were examined. In addition to measuring the mechanical properties of these sandwich-type samples, predictions of the moduli of multi-material samples were made based on the properties of the individual materials. The fundamentals of the calculation and design of sandwich structures can be found in detail in.[13] The calculation of the stiffnesses and stresses of symmetrical sandwich structures under tension and bending is central to this work and is briefly outlined here (equations are taken from Reference [13]).

Under tensile load, a bar is assumed with a geometry defined by its length and a constant cross-sectional area, deforming only in the longitudinal direction. Although the assumption of a constant area is limited in reality due to necking effects, it is employed for simplicity in this calculation. Material behavior is described by the one-dimensional Hooke's law (Equation (1)), where E represents Young's modulus, σ is the normal stress and ε is the strain. The stress is induced by an external normal force.

$$E = \frac{\sigma}{\varepsilon}. \tag{1}$$

For a composite material consisting of n parallel layers arranged in the tensile direction, the average tensile stiffness $\overline{EA}$ can be calculated using Equation (2). E_k, h_k, and w_k represent Young's modulus, height, and width of the individual layer k.

$$\overline{EA} = \sum_{k=1}^{n} E_k \Delta h_k w_k. \tag{2}$$

This study focuses on symmetrical sandwich structures, as illustrated in Figure 2. The samples consist of two shell layers with a Young's modulus E_s and a height

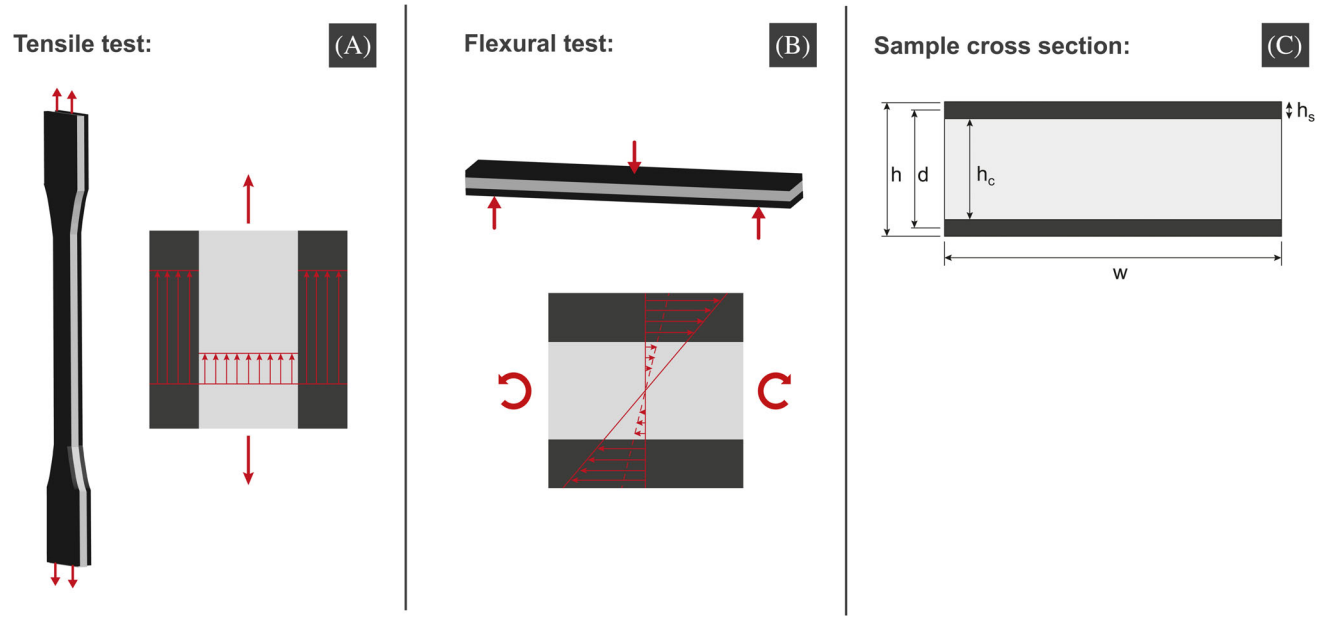

FIGURE 2 (A) Tensile test sample and schematic stress distribution. (B) Flexural test sample and schematic stress distribution. (C) Cross-section of samples with a description of geometry variables.

of h_s and one core layer with a Young's modulus E_c and a height of h_c. The width of the individual layers is equal to the width w of the overall sample. The stiffness $\overline{EA}$ can then be calculated using Equation (3).

$$\overline{EA} = 2E_s h_s w + E_c h_c w. \tag{3}$$

The prediction of the Young's modulus E_{Sandwich} of the sandwich sample can be done using the overall sample cross-section

$$A_{Sandwich} = h \cdot w = (2h_s + h_c) \cdot w \tag{4}$$

and the simplification, that the layer heights h_s and h_c depend only on the volume fractions of the shell material φ_s and the core material φ_c:

$$h_s = \frac{1}{2} h \cdot \varphi_s \text{ and } h_c = h \cdot \varphi_c. \tag{5}$$

This leads to Equation (6), with calculates the total Young's modulus E_{Sandwich} based on the volume fractions of the components, similar to the rule of mixture, generally known from composites.[35]

$$E_{\text{Sandwich}} = E_s \cdot \varphi_s + E_c \cdot \varphi_c. \tag{6}$$

Additionally to the investigation of the material stiffness, the stress distribution, illustrated in Figure 2, will be analyzed to gain insights into sample failure. It should be noted that the figure simplifies the stress distribution by omitting shear stress. Equation (7) is used to calculate the stress σ_k in the k^{th} layer, considering the normal force F_0, that is applied to the overall sample.

$$\sigma_k = \frac{F_0 E_k}{\overline{EA}}. \tag{7}$$

The theory for the flexural test is based on a bending beam, which is loaded and deformed only perpendicular to its longitudinal axis, with individual forces perpendicular to the longitudinal axis or moments occurring as external forces.

The simplest case is described by the Euler-Bernoulli theory,[13] which assumes that shear stresses have no influence on the deformation. Strictly speaking, this assumption can only be used for slender, homogeneous beams with L> > h. More complex models are provided by Timoshenko[36] or Levinson,[37] but these are not considered in detail here.

For sandwich structures, the beam theory, according to Euler-Bernoulli, can be employed for simplification. According to this theory, the average bending stiffness $\overline{EI_y}$ is generally calculated as shown in Equation (8).

$$\overline{EI_y} = \sum_{k=1}^{3} E_k \left[\frac{1}{12} \mathrm{w} \cdot (h_k)^3 + b h_k \cdot \left(z_c^k\right)^2 \right] = \sum_{k=1}^{3} E^k I_y^k. \tag{8}$$

The total bending stiffness $\overline{EI_y}$ results from the sum of the moduli of elasticity E_k of the individual layers and

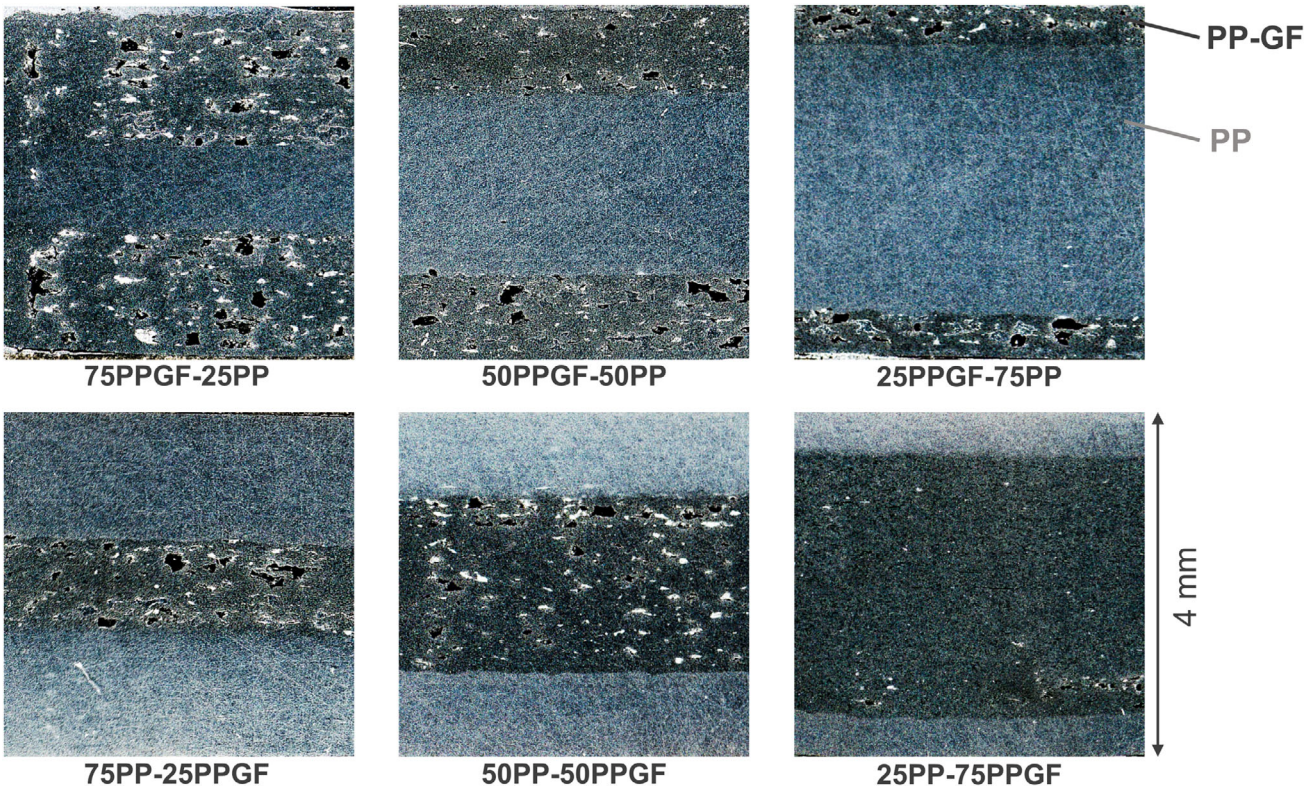

FIGURE 3 Microscopic pictures of cross-sections of all sandwich tensile bars. Light gray: polypropylene (PP), dark gray: glass fiber-filled polypropylene (PPGF)PPGF.

the area moments of inertia I_y^k. Here, w denotes the width of the bending beam, h_k the height of a layer and z is the distance of the partial center of gravity of the layer to the total center of gravity of the body. For a homogeneous layer, the formula is simplified to Equation (9):

$$\overline{EI_y} = E\frac{1}{12}wh^3 \tag{9}$$

For a symmetrical sandwich structure with identical shell layers (Figure 2), Equation (10) results for the overall bending stiffness of the composite:

$$\overline{EI_y} = \frac{(E_S \cdot \mathrm{w} \cdot h_S^3)}{6} + \frac{(E_S \cdot \mathrm{w} \cdot h_S \cdot d^2)}{2} + \frac{(E_C \cdot \mathrm{w} \cdot h_C^3)}{12}. \tag{10}$$

In this equation, the first term represents the stiffness of the shell layers, the third term the stiffness of the core and the second term the so-called Steiner component, which takes into account the influence of the stiffness of the shell layers relative to their distance d to the overall center of gravity of the structure.

The subsequent results primarily rely on Equations (6), (7) and (10). The calculations of the sandwich-type samples are done using the measured mechanical values of the printed individual materials PP and PPGF.

3 | RESULTS AND DISCUSSION

3.1 | Structural properties

Micrographs of all sandwich-type composites are depicted in Figure 3. The lighter color represents the PP material. Good printing quality without pores can be seen here. In contrast, the darker areas, representing the PPGF phase, exhibit a notable presence of pores evenly distributed across the PPGF layers. The higher viscosity at processing temperature due to the higher melting temperature (see data sheet[34]) and the lower mobility of the chains due to the obstruction by glass fibers most likely contribute to the larger number of pores in PPGF. New melted material can hardly flow into the pores of the underlying layers and fill them. Despite imperfect printing quality, reproducibility for all samples is maintained. In addition, no delamination between the layers, particularly at the PP-PPGF interface, can be detected. Good symmetry was achieved.

3.2 | Tensile properties

The results of the tensile tests are presented in Table 4. 100PP shows the lowest Young's modulus of 497 ± 39 MPa, while 100PPGF has the highest value of 2910 ± 162 MPa.

	Young's modulus (MPa)	Tensile strength (MPa)	Elongation at break (%)
100PP	497 ± 39	17.9 ± 0.2	>100[a]
75PP-25PPGF	1241 ± 26	24.5 ± 0.6	11.3 ± 1.2
50PP-50PPGF	1777 ± 41	28.3 ± 0.9	6.0 ± 0.4
25PP-75PPGF	2229 ± 35	31.6 ± 1.8	4.2 ± 0.8
100PPGF	2910 ± 162	43.3 ± 0.8	4.0 ± 0.4
75PPGF-25PP	2180 ± 72	31.1 ± 0.9	4.7 ± 0.5
50PPGF-50PP	1634 ± 38	25.7 ± 0.5	5.8 ± 0.7
25PPGF-75PP	1182 ± 15	23.4 ± 0.4	12.6 ± 0.8

[a]No fracture until end of measurement at 100% elongation.

TABLE 4 Results from tensile test: average value and sample standard deviations for Young's modulus, tensile strength and elongation at break of all samples.

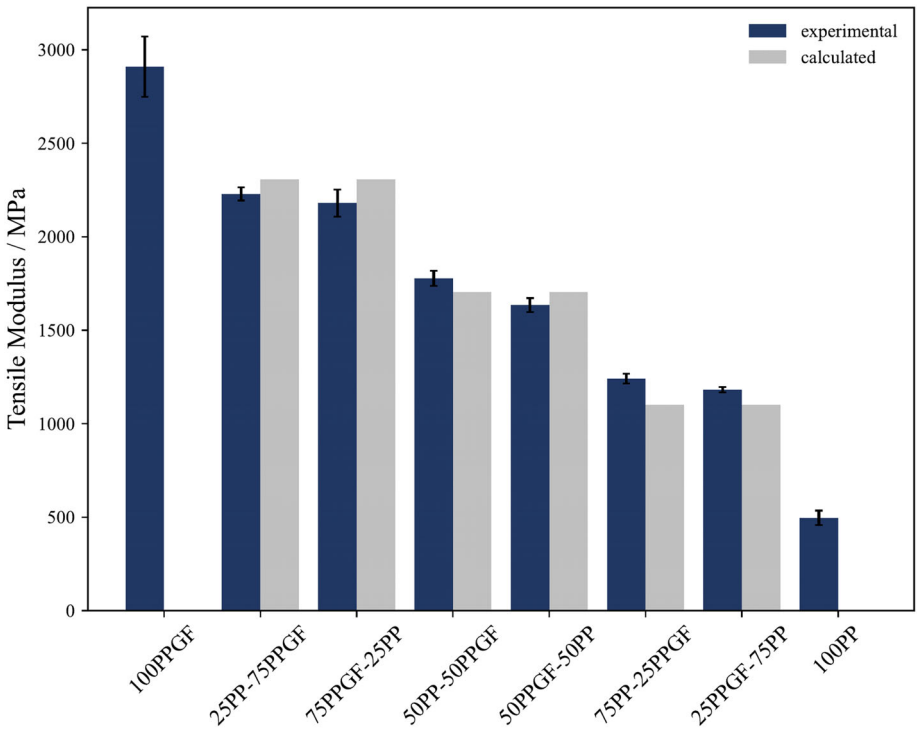

FIGURE 4 Experimental versus calculated data of Young's modulus (calculations are based on measured values of polypropylene (PP) and glass fiber-filled polypropylene (PPGF)).

The measured values for tensile strength were 17.9 ± 0.2 MPa and 43.3 ± 0.8 MPa for 100PP and 100PPGF, respectively. All values slightly exceed those given in the data sheets and have a low standard deviation, indicating high reproducibility. This behavior is essential as a basis for subsequent calculations.

In the sandwich-type composites, Young's modulus increased continuously with increasing PPGF content. Notably, the order of the layers has no significant influence, but only the content of the two materials impacts stiffness. This behavior is in good agreement with the theory presented in Section 2.4. To prove that Equation (6) is valid, the experimental and calculated values of Young's modulus are compared in Figure 4. A maximum deviation of 11% is observed for 75PP-25PPGF, whereas all other deviations remain below 7%. These findings suggest a high degree of predictability for Young's modulus in printed sandwich-type composites based on the moduli of the individual materials.

The tensile strength exhibits a trend similar to the modulus. A higher content of PPGF correlates with an increased tensile strength. In this case, the dependency is slightly below a linear correlation. The elongation at break differs significantly between PPGF and PP, ranging from 4% to over 100%. Even a modest amount of 25% PPGF results in a sharp drop in elongation at break to approximately 12%, related to the high stiffness of the PPGF material hindering extensive plastic deformation. Moreover, it can be seen that elongation at break remains consistent for the samples with equal amounts of the two materials, irrespective of layer order.

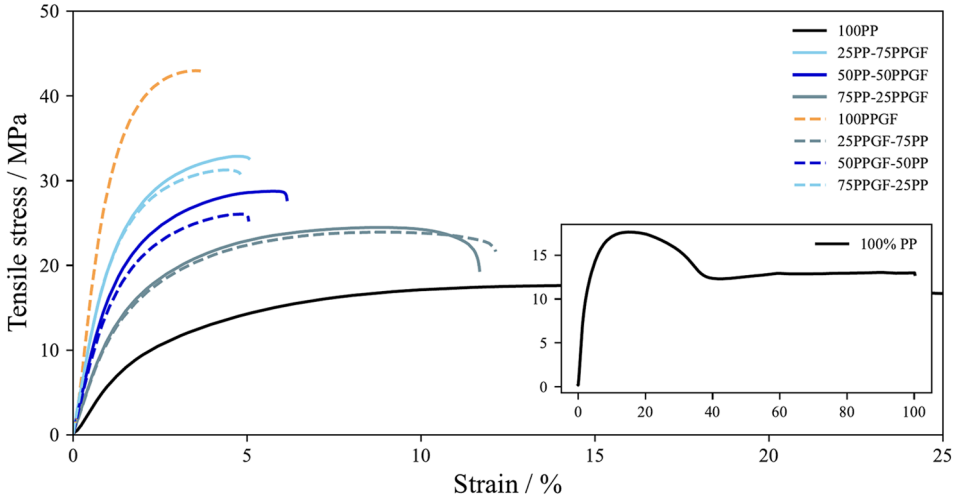

FIGURE 5 Representative stress–strain curves of all materials tested in tensile mode. Same color = same material amounts, solid line = PP as shell layer, dashed line = PPGF as shell layer.

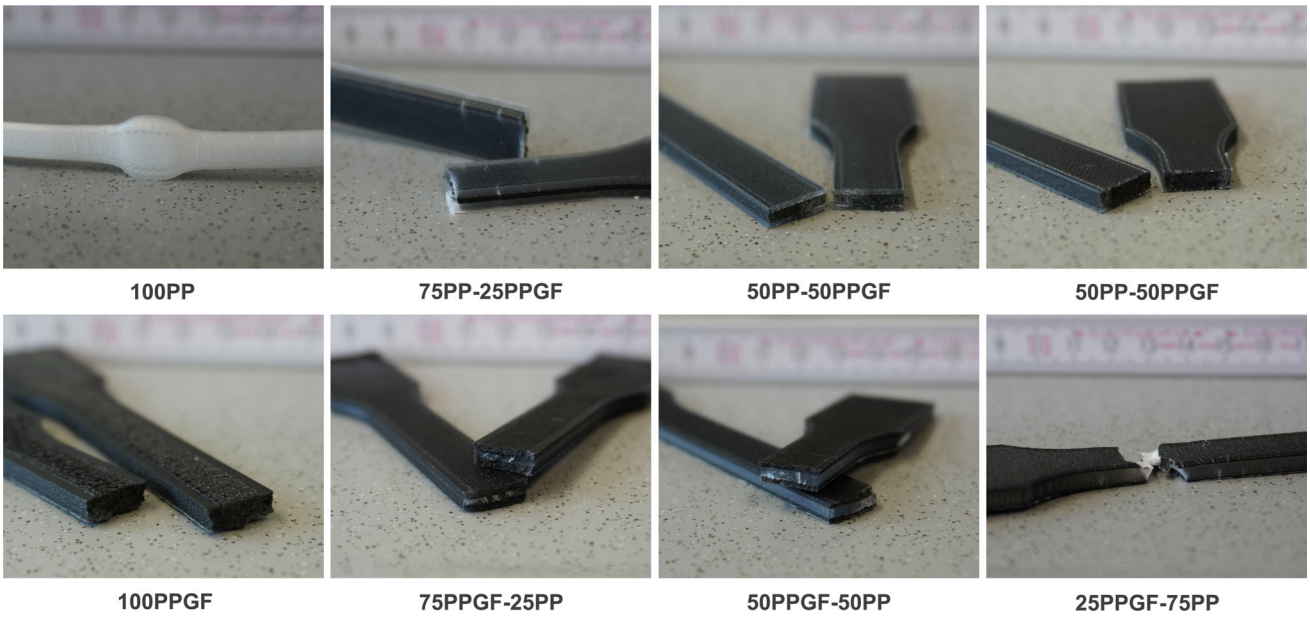

FIGURE 6 Images of tensile bars after testing. White phase represents PP, black phase represents PPGF.

A closer look at the stress–strain curves in Figure 5 and at the samples after testing in Figure 6 provides insights into the failure behavior of the specimens. PP undergoes early-stage plastic deformation, resulting in necking which is visible as a drop in the stress–strain-curve. Eventually, elongation exceeds 100% strain. In contrast, all other specimens demonstrate a predominantly brittle fracture, with a maximum strain of 12% and a smooth fracture surface. However, a higher amount of PP can increase the elongation at break of the sandwich composite. To explain the observed phenomenon, it is worth looking at the PPGF25-PP75 and PP75-PPGF25 specimens, both comprising 75% PP and 25% PPGF. Small cracks can be detected in the pictures of the fractured samples in Figure 6. These cracks originate in the PPGF phase and are also present in other compositions, but not as pronounced. When the sandwich-type composite reaches a critical level of strain, cracks initiate in the PPGF phase. For the 100% PPGF samples, this leads to immediate failure of the tensile bars. In the sandwich-type composites there exists a distinct stress distribution between PP and PPGF.

To estimate the stress distribution, Equation (7) was used to calculate the stresses in PP and PPGF, based on the average stress values derived from the measured curves of all samples. For this purpose, four different cases were examined with respect to the stresses occurring within the specimens. Figure 8 illustrates the four

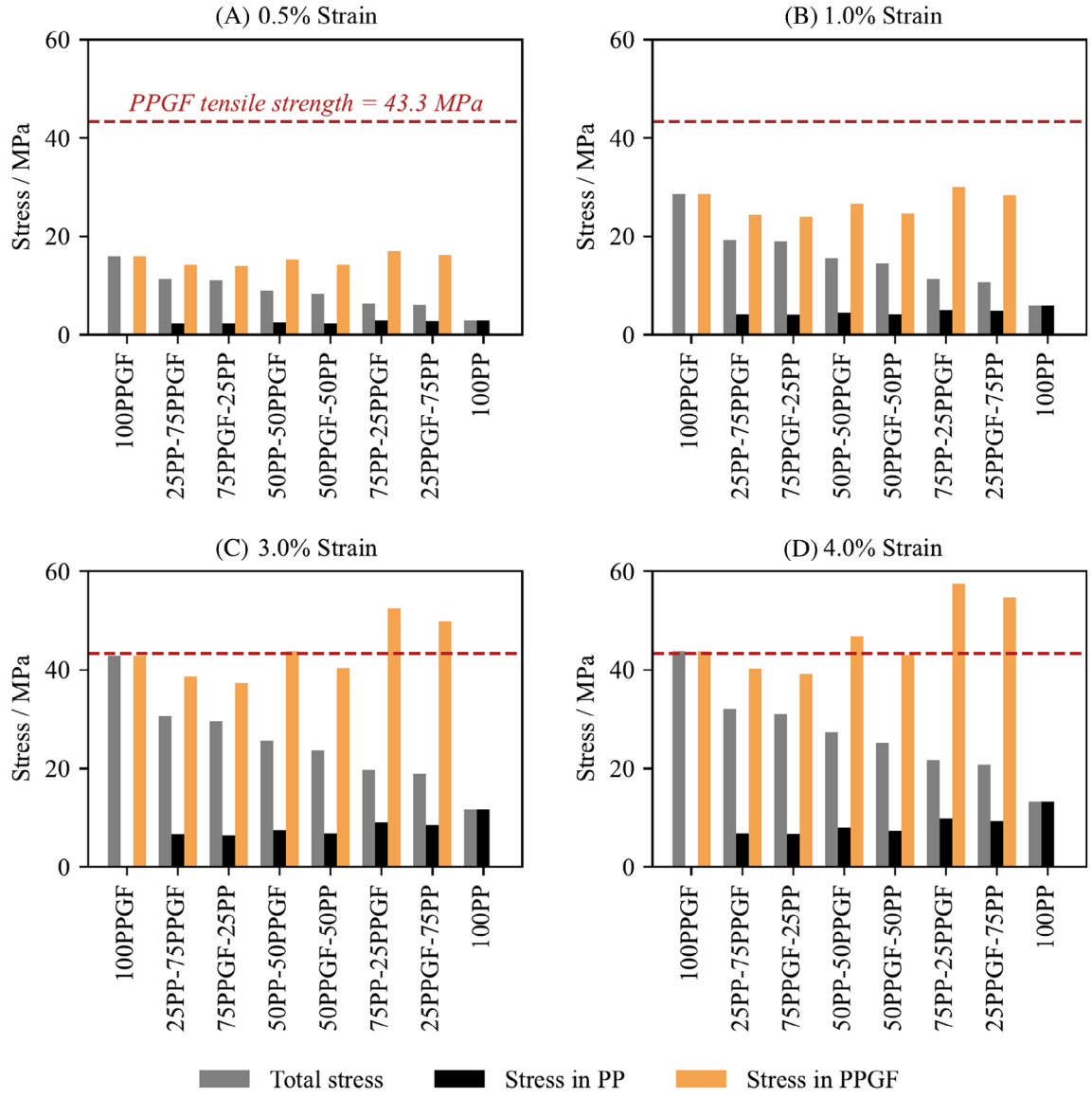

FIGURE 7 Average experimentally measured total stress values (gray) in sandwich composites at defined strains (0.5%, 1%, 3%, and 4%) and calculated stress distribution between polypropylene (PP) (black) and PPGF (orange) for each sandwich type. The red line indicates the tensile strength of glass fiber-filled polypropylene (PPGF), theoretically leading to the failure of the PPGF contents in the sandwich composites.

selected strain levels. At 0.5%, a linear-elastic behavior is given. At 1%, the deformation behavior transitions from fully elastic to initial plastic deformation. At 3%, plastic deformation continues while PP as well as PPGF are still intact based on the individual materials. The final stage of 4% strain represents the point at which PPGF already fails, while PP is still intact. Figure 7 shows the stress distributions at these four different strain levels.

At 0.5% (Figure 7A) and 1% (Figure 7B) strain, the stresses are low in both PP and PPGF. The deformation behavior is mainly linear elastic at these levels. However, at a strain of 3% (Figure 7C), the stresses in the PPGF phase for the three sandwich materials 50PP-50PPGF, 75PP-25PPGF and 25PPGF-75PP reach a critical level. In Figure 7C it can be seen that the red line, standing for the tensile strength of neat PPGF, is reached or even exceeded. Consequently, cracks develop in the PPGF phase. At the same time, the calculated stresses in the PP phase remain comparatively low according to the model. For 4% strain (Figure 7D) the calculated stresses in PPGF further increase, now leading to failure of the PPGF phase in the 50PPGF-50PP samples.

These theoretical investigations align with the observed failure patterns in the tensile tests. When subjected to tensile load, the majority of stress is borne by the PPGF phase due to its higher modulus. Depending on

the material composition, at a certain strain, the tensile strength of PPGF is reached and cracks develop. Contrary to the initial assumption that 3% strain is not critical for PPGF because neat PPGF can withstand this strain, critical stresses arise in the sandwich-type specimen at this stage.

At equal strain, the stress in the material with a lower amount of PPGF is higher, leading to early crack development and propagation through the PPGF layers, as observed in Figure 6. These cracks propagate to some extent into the PP phase, causing local stress concentrations and much higher stresses as estimated in Figure 7 for the PP phase. Due to its ductility, PP can absorb stress through deformation, ultimately resulting in strain hardening and the formation of white spots, as visible in Figure 6. This phenomenon enables a crack-stopping effect in PP. However, the initial stability of the PPGF layers is compromised, only a low part of its stiffness can further be utilized by shear forces between PP and PPGF. Interestingly, even when cracks initiate in PPGF at 3% strain, the elongation at break of the two sandwich-type materials remains relatively high at 11.6% and 12.8%. Similarly the materials with 50% PP and 50% PPGF, critical stress occurs in PPGF at 4% strain, yet the elongation at break is 5.8% and 6.0%. This highlights the ability of the PP phase to serve as a crack-bridging layer, preventing catastrophic failure. It also indicates a good adhesion between PP and PPGF. Without such adhesion, delamination would likely occur when the crack reaches the PP-PPGF interface.

In conclusion, the tensile behavior of sandwich-type composites of PP and PPGF can be accurately predicted and correlated with the behavior of the two individual materials. This suggests a high potential for tailoring the mechanical properties of composite parts by blending the properties of both materials.

TABLE 5 Results from flexural test: average value and sample standard deviations for flexural modulus and flexural strength of all samples.

	Flexural modulus (MPa)	Flexural strength (MPa)
100PP	683 ± 5	24.9 ± 0.4
75PP-25PPGF	739 ± 22	27.2 ± 0.6
50PP-50PPGF	1000 ± 43	35.6 ± 0.7
25PP-75PPGF	1759 ± 78	49.7 ± 1.0
100PPGF	3182 ± 76	64.8 ± 1.5
75PPGF-25PP	3105 ± 136	62.7 ± 1.4
50PPGF-50PP	2949 ± 110	57.0 ± 2.2
25PPGF-75PP	2113 ± 106	42.2 ± 1.0

3.3 | Flexural properties

The results of the flexural tests are summarized in Table 5. Similar to the tensile behavior, a significant difference is observed between the moduli of 100PP, measured at 683 ± 5 MPa, and 100PPGF measured at 3182 ± 76 MPa. However, the bending behavior of the sandwich-type composites differs markedly from the previous findings under tensile load. While specimens with the same material composition show similar moduli in tensile mode, the flexural moduli of samples with PPGF as the shell material are notably higher than those with PP in the shell. The contents of both phases

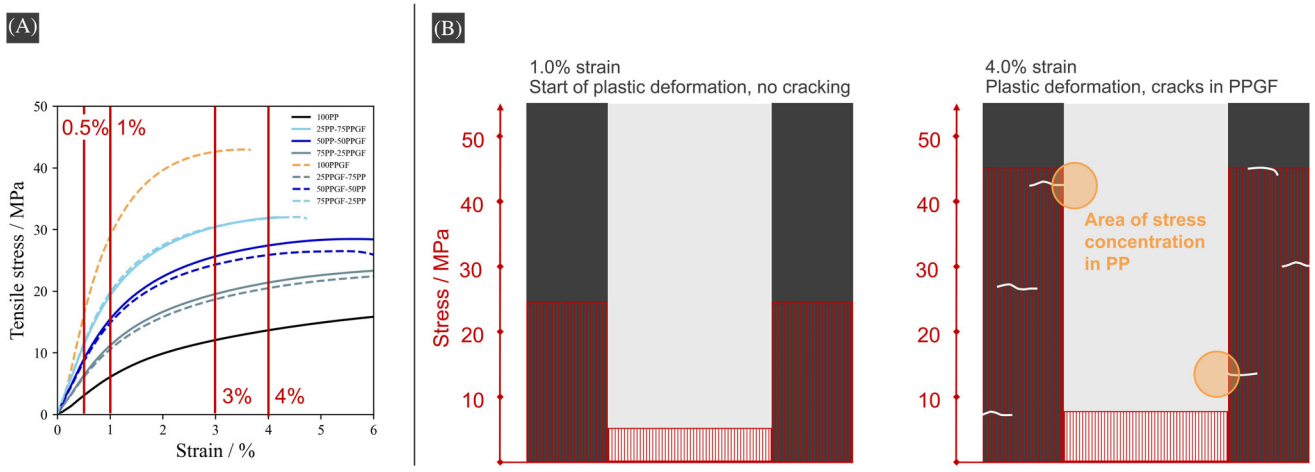

FIGURE 8 (A) Stress–strain-diagram with marked strain levels: 0.5%—linear elastic region, 1%—transition from linear-elastic to plastic deformation, 3% plastic deformation without fracture, 4% plastic deformation, partial fracture of glass fiber-filled polypropylene (PPGF) phase. (B) Illustration of stress distribution between polypropylene (PP) and PPGF in PPGF50-PP50 with cracks occurring at 4.0% strain.

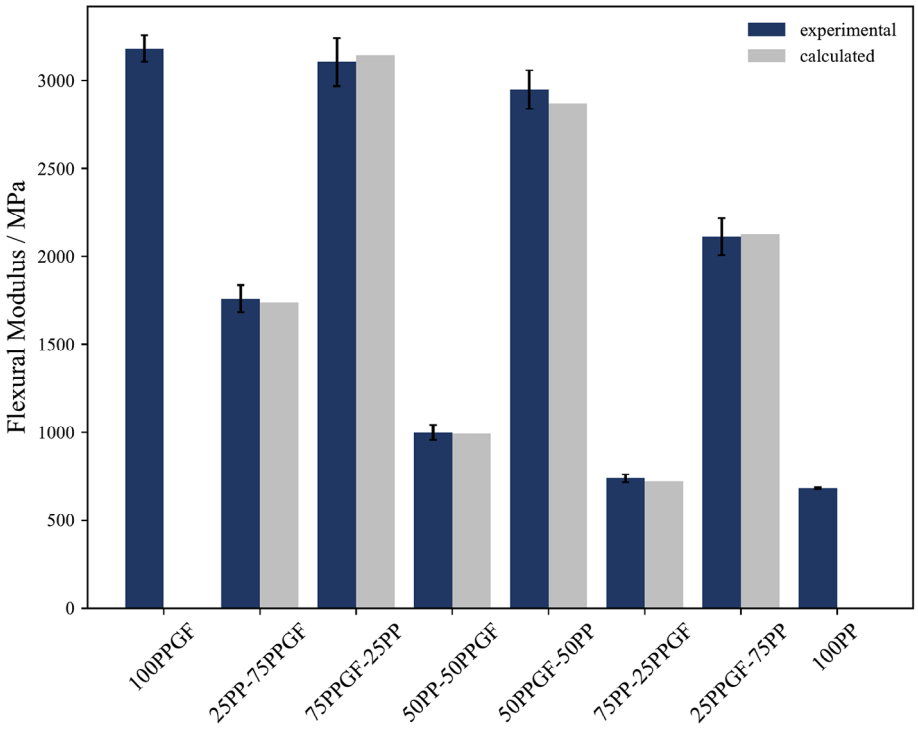

FIGURE 9 Experimental versus calculated data of flexural modulus (calculated data are based on single polypropylene (PP) and glass fiber-filled polypropylene (PPGF) values).

have a minor effect on the flexural modulus and strength. This observation is consistent with the sandwich theory addressed in Section 2.4. As long as the shell material is present in a larger proportion, the term for the stiffness of the core layer from Equation (3) has a minor influence on the overall stiffness of the specimen. In particular, for the PPGF50-PP50 specimens, an average flexural modulus of 2949 MPa was measured, equivalent to 93% of the stiffness of neat PPGF. Efficient stiffening of the samples can be achieved with PPGF as a shell material. Additionally, an interesting observation can be made comparing the results with a study on injection-molded sandwich structures, Loypetch et al. present on the injection molding of a (foamed) PP core between short-fiber reinforced skin layers. A sample composed of a compact PP core and two skin layers with 30% of glass fibers in PP (representing 20% of the sandwich structure) showed an almost threefold increase in modulus.[38] This result aligns excellently with the findings for the 25PPGF-75PP sample presented here. This comparison demonstrates that the printing process does not weaken the material when compared to this injection molding study.

To confirm the validity of the sandwich theory for the materials studied, Figure 9 compares the calculated and experimental data for the flexural modulus. The values are in excellent agreement. The maximum deviation between the measured and calculated flexural modulus is only 3%, which falls within the standard deviation of the measured data. This behavior is particularly interesting as, despite the porosity present within the samples, a good prediction is feasible. Additionally, the layer adhesion in PP, PPGF and between both materials is sufficient to withstand the shear forces that occur under flexural load at low deformations.

Further insides into the failure mode are provided by the stress-deformation curves in Figure 10 and the microscopic images of the specimen after testing in Figure 11. All specimens with a PPGF shell fail at a deformation between 5% and 7%.

The images of the fractured specimens in Figure 11 reveal that this failure initiates with crack formation in the PPGF shell. The crack originates in the bottom layer under tensile load when the tensile elongation at break of the outer layer is reached. Subsequently, the crack propagates through all PPGF layers, leading to the sample failure. Similar to the tensile mode, the crack is stopped in the PP phase by plastic deformation. However, the bottom layer remains critical for the failure of the specimen.

For all samples with PP in the shell, a deformation of 11%–16% is reached. It should be considered that this is actually not the breaking deformation, as no distinct cracks or damage can be observed for those samples in Figure 11. The maximum deformation is determined by the settings of the measurements. The PP shell is capable of sustaining high strains while dissipating energy through plastic deformation. Since specimens with a length of 80 mm and a spacing of 64 mm were used, failure by cracking cannot be reached within the test setup. A stop criterion of a drop of 20% in force was defined. Therefore, the maximum measured deformation is not equal to the deformation at break and no final conclusion

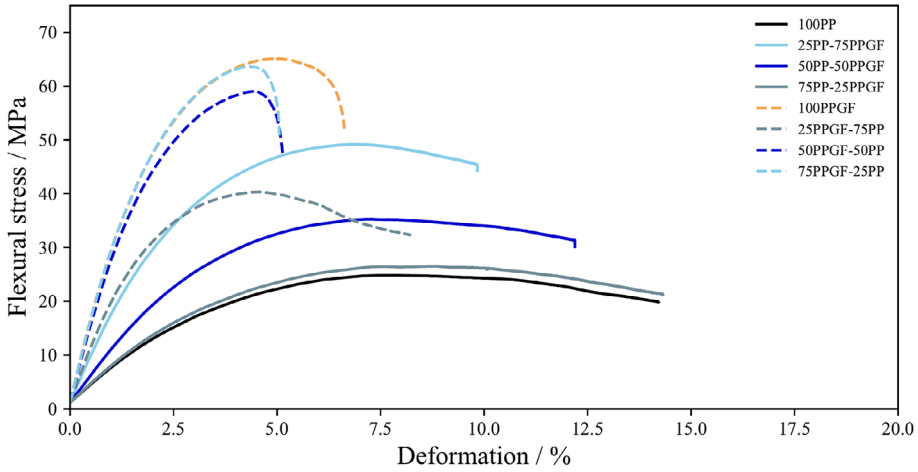

FIGURE 10 Representative stress–strain curves of all materials tested in flexural mode. Same color = same material amounts, solid line = PP as shell layer, dashed line = PPGF as shell layer.

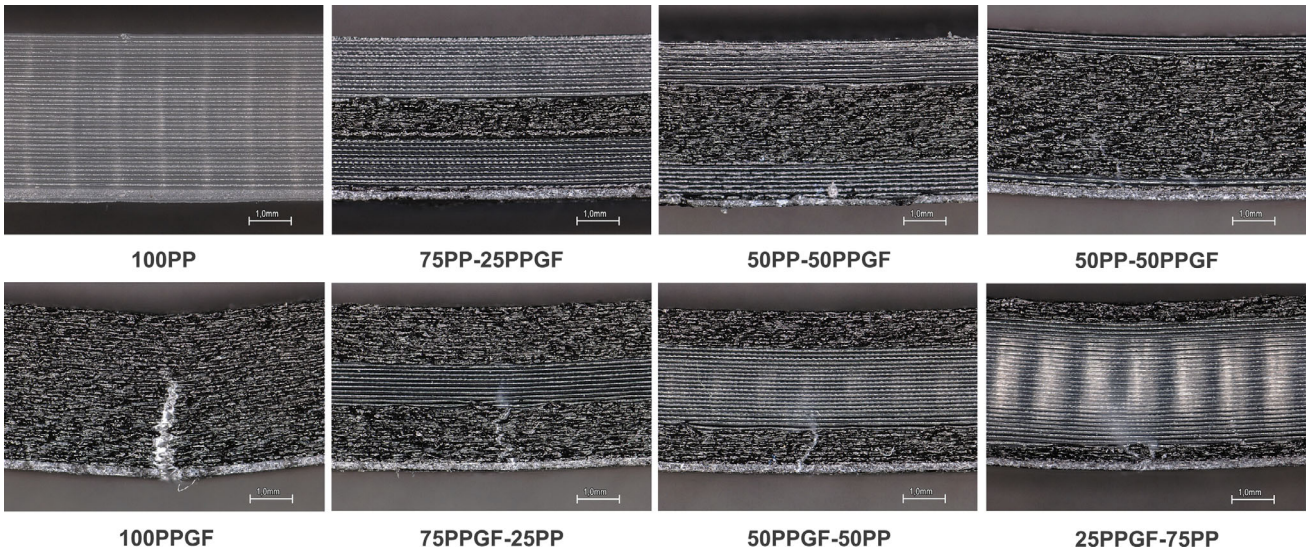

FIGURE 11 Microscopic pictures of side view of flexural bars after testing. Cracks can be detected in bottom layers when glass fiber-filled polypropylene (PPGF) is shell material.

can be drawn regarding the failure mode for the samples with PP as shell material. However, a closer look at the interface between PP and PPGF reveals some "waviness", indicating delamination at this point. This delamination is caused by shear forces between the layers at high deformations, attributed to the differing deformability of PP and PPGF, which leads to high shear forces at the interface.

While a detailed study of this effect is still pending, it can be assumed that two different failure modes occur depending on the shell material. When PPGF is in the shell, it leads to tensile failure in the bottom layer, followed by crack propagation through the PPGF layers, which can only be stopped by plastic deformation in the PP phase. On the other hand, when PP is the shell layer, the tensile and compressive stresses in the shell are not as critical because they can be reduced by plastic deformation and energy dissipation. Therefore, the materials with PP as a shell will not fail by breaking but rather by a deformation that would be critical in any application.

4 | CONCLUSION

In this study, the mechanical behavior of 3D-printed PP-PPGF sandwich-type composites was investigated and correlated to theoretical models.

Firstly, it was proved that PP and PPGF exhibited good adhesion, allowing high and reproducible quality when joining them in a sandwich structure. It was demonstrated that ductile PP and stiff PPGF, with a modulus 5–6 times higher, can be combined into composites covering the entire range of moduli between the two base materials. The comparison with the theoretical calculation shows excellent agreement, with an average difference of only 6% in tensile mode and 1.4% in flexural mode. Therefore, providing a strong foundation for reliable predictions is provided.

Furthermore, PP-PPGF composites offer the ability to tailor the deformation and failure behavior by distributing stress between both materials. While PPGF

content not only increases the modulus but also the tensile and flexural strength, PP provides a crack-bridging effect, preventing premature failure and increasing elongation at break. Stress distribution calculations, based on the measured results, could be brought into context with crack propagation and failure mechanisms of shell and core layer.

In conclusion, the investigated PP-PPGF sandwich-type composites offer effective tailoring and prediction of mechanical properties through multi-material printing. Future research could explore whether these mechanical properties can also be accurately predicted for more complex geometries using numerical simulations. Exploring how printing patterns and orientations influence adhesion and mechanical behavior is another important avenue. Additionally, examining other load cases, dynamic mechanical properties, and the long-term performance of printed multi-material components will provide valuable insights for technical applications.

AUTHOR CONTRIBUTIONS

Julia Utz: conceptualization, methodology, visualization, formal analysis, data curation, writing – original draft. **Amelie Ferbert:** investigation, visualization, writing – original draft. **Nico Geis:** validation, writing – review & editing. **Holger Ruckdäschel:** supervision, writing – review & editing.

ACKNOWLEDGMENT

Open Access funding enabled and organized by Projekt DEAL.

FUNDING INFORMATION

This work was funded by the Open Access Publishing Fund of the University of Bayreuth.

CONFLICT OF INTEREST STATEMENT

The authors declare that they have no known competing financial interests or personal relationships that could have appeared to influence the work reported in this paper.

DATA AVAILABILITY STATEMENT

The data that support the findings of this study are available from the corresponding author upon reasonable request.

ORCID

Julia Utz https://orcid.org/0000-0001-5486-9682
Nico Geis https://orcid.org/0000-0003-0647-3178
Holger Ruckdäschel https://orcid.org/0000-0001-5985-2628

REFERENCES

1. Inamdar A, Magana M, Medina F, Grajeda Y, Wicker R. Development of an automated multiple material stereolithography machine. Paper presented at international solid freeform fabrication symposium. 2006.
2. Choi J-W, MacDonald E, Wicker R. Multi-material microstereolithography. *Int J Adv Manuf Technol*. 2009;49(5–8):543-551.
3. Laumer T, Stichel T, Amend P, Schmidt M. Simultaneous laser beam melting of multimaterial polymer parts. *J Laser Appl*. 2015;27(S2):S29204. doi:10.2351/1.4906303
4. Chen T, Mueller J, Shea K. Integrated design and simulation of tunable, multi-state structures fabricated monolithically with multi-material 3D printing. *Sci Rep*. 2017;7:45671.
5. Keating SJ, Gariboldi MI, Patrick WG, Sharma S, Kong DS, Oxman N. 3D printed multimaterial microfluidic valve. *PLoS One*. 2016;11(8):e0160624.
6. Rafiee M, Farahani RD, Therriault D. Multi-material 3D and 4D printing: a survey. *Adv Sci Weinh*. 2020;7(12):1902307.
7. Saadi M, Maguire A, Pottackal NT, et al. Direct ink writing: a 3D printing technology for diverse materials. *Adv Mater*. 2022;34(28):e2108855.
8. García-Collado A, Blanco JM, Gupta MK, Dorado-Vicente R. Advances in polymers based multi-material additive-manufacturing techniques: state-of-art review on properties and applications. *Addit Manuf*. 2022;50:102577.
9. Baca Lopez DM, Ahmad R. Tensile mechanical behaviour of multi-polymer Sandwich structures via fused deposition modelling. *Polymers*. 2020;12(3):651. doi:10.3390/polym12030651
10. Baca D, Ahmad R. The impact on the mechanical properties of multi-material polymers fabricated with a single mixing nozzle and multi-nozzle systems via fused deposition modeling. *Int J Adv Manuf Technol*. 2020;106(9–10):4509-4520.
11. Moghanizadeh A, Ashrafizadeh F. Studying sacrificial ice structure, as soluble support layers, in 3D printing of polymers (FDM). *Prog Addit Manuf*. 2021;6(4):757-763.
12. Nazir A, Gokcekaya O, Md Masum Billah K, et al. Multi-material additive manufacturing: a systematic review of design, properties, applications, challenges, and 3D printing of materials and cellular metamaterials. *Mater Des*. 2023;226:111661.
13. Öchsner A. *Mechanics of Classical Sandwich Structures*. Springer; 2023.
14. Allen HG, Neal BG. *Analysis and Design of Structural Sandwich Panels*. Pergamon; 1969.
15. Nanko M. Definition and categories of hybrid materials. *J Mater*. 2009;11:1-8.
16. Arifvianto B, Satiti BE, Salim UA, Suyitno, Nuryanti A, Mahardika M. Mechanical properties of the FFF sandwich-structured parts made of PLA/TPU multi-material. *Prog Addit Manuf*. 2022;7(6):1213-1223.
17. Yilmaz S, Gul O, Eyri B, Karsli NG, Yilmaz T. Analyzing the influence of multimaterial 3D printing and postprocessing on mechanical and tribological characteristics. *Macromol Mater Eng*. 2024;309(5):2300428. doi:10.1002/mame.202300428
18. Kim H, Park E, Kim S, Park B, Kim N, Lee S. Experimental study on mechanical properties of single- and dual-material 3D printed products. *Procedia Manuf*. 2017;10:887-897.
19. Lopes LR, Silva AF, Carneiro OS. Multi-material 3D printing: the relevance of materials affinity on the boundary interface performance. *Addit Manuf*. 2018;23:45-52.

20. Rabbi MF, Chalivendra V. Interfacial fracture characterization of multi-material additively manufactured polymer composites. *Compos Part C: Open Access*. 2021;5:100145.
21. Yin J, Lu C, Fu J, Huang Y, Zheng Y. Interfacial bonding during multi-material fused deposition modeling (FDM) process due to inter-molecular diffusion. *Mater Des*. 2018;150:104-112.
22. Lin W, Shen H, Xu G, Zhang L, Fu J, Deng X. Single-layer temperature-adjusting transition method to improve the bond strength of 3D-printed PCL/PLA parts. *Compos Part A: Appl Sci Manuf*. 2018;115:22-30.
23. Andó M, Birosz M, Jeganmohan S. Surface bonding of additive manufactured parts from multi-colored PLA materials. *Measurement*. 2021;169:108583.
24. Dairabayeva D, Perveen A, Talamona D. Investigation on the mechanical performance of mono-material vs multi-material interface geometries using fused filament fabrication. *Rapid Prototyp J*. 2023;29(11):40-52.
25. Ribeiro M, Sousa Carneiro O, Ferreira da Silva A. Interface geometries in 3D multi-material prints by fused filament fabrication. *Rapid Prototyp J*. 2019;25(1):38-46.
26. Nasirov A, Hasanov S, Fidan I. Prediction of mechanical properties of fused deposition modeling made parts using multiscale modeling and classical laminate theory. Paper Presented at 2019 International Solid Freeform Fabrication Symposium. 2019.
27. Mishra PK, Senthil P. Prediction of in-plane stiffness of multi-material 3D printed laminate parts fabricated by FDM process using CLT and its mechanical behaviour under tensile load. *Mater Today Commun*. 2020;23:100955.
28. Cuan-Urquizo E, Barocio E, Tejada-Ortigoza V, Pipes RB, Rodriguez CA, Roman-Flores A. Characterization of the mechanical properties of FFF structures and materials: a review on the experimental, computational and theoretical approaches. *Materials*. 2019;12(6):895. doi:10.3390/ma12060895
29. Sharafi S, Santare MH, Gerdes J, Advani SG. A multiscale modeling approach of the fused filament fabrication process to predict the mechanical response of 3D printed parts. *Addit Manuf*. 2022;51:102597.
30. Sam-Daliri O, Ghabezi P, Steinbach J, et al. Experimental study on mechanical properties of material extrusion additive manufactured parts from recycled glass fibre-reinforced polypropylene composite. *Compos Sci Technol*. 2023;241:110125.
31. Utz J, Geis N, Baur M, Ruckdäschel H. Influence of glass fibers on the processability and mechanical properties of PP homopolymer for fused filament fabrication (FFF). *AIP Conf Proc*. 2023;2607(1):120009.
32. Sodeifian G, Ghaseminejad S, Yousefi AA. Preparation of polypropylene/short glass fiber composite as fused deposition modeling (FDM) filament. *Results Phys*. 2019;12:205-222.
33. BV BDPS. Technical Data Sheet—Ultrafuse PP. Version No. 4.0. 2020.
34. BV BDPS. Technical Data Sheet—Ultrafuse PP GF30. Version No. 2.3. 2019.
35. Ashby MF. *Materials Selection in Mechanical Design*. Elsevier Science; 2016.
36. Timoshenko SP. LXVI. On the correction for shear of the differential equation for transverse vibrations of prismatic bars. *Lond Edinb Dubl Philos Mag*. 1921;41(245):744-746.
37. Levinson M. A new rectangular beam theory. *J Sound Vib*. 1981;74(1):81-87.
38. Loypetch N, Tröltzsch J, Nestler D, Kroll L, Siengchin S. Thermoplastic foam injection moulding of sandwich structures with short fibre-reinforced skin layers. *J Sandw Struct Mater*. 2019;23(1):301-321.

How to cite this article: Utz J, Ferbert A, Geis N, Ruckdäschel H. Mechanical properties and predictive analysis of multi-material polypropylene-glass fiber sandwich structures produced by material extrusion. *Polym Compos*. 2025;46(11):10239-10253. doi:10.1002/pc.29617